PHYSICAL REVIEW B VOLUME 7, NUMBER 6 15 MARCH 1973

Optical Properies of Graphite*

L. G. Johnson†
Department of Electrical Engineering, Massachusetts Institute of Technology, Cambridge, Massachusetts 02139
and Lincoln Laboratory, Massachusetts Institute of Technology, Lexington, Massachusetts 02173

G. Dresselhaus
Lincoln Laboratory, Massachusetts Institute of Technology, Lexington, Massachusetts 02173
(Received 23 August 1972)

A three-dimensional Fourier expansion has been developed to describe the dispersion relations $E(\vec{k})$ for the π bands of graphite throughout the Brillouin zone. The coefficients of the Fourier expansion are evaluated by a fit to the experimentally determined parameters of the Slonczewski–Weiss model, as well as to the optical data. Using this energy-band model, the interband contribution to the frequency-dependent dielectric constant has been calculated in the energy range $0.5 < \hbar\omega < 6$ eV for both $\vec{E} \perp \vec{c}$ and $\vec{E} \parallel \vec{c}$. For this calculation, a numerical-integration procedure has been developed to carry out the full-zone integrations. The results for the dielectric constant are primarily dependent on the values of the McClure parameters γ_0, γ_1, γ_3, and γ_4, which enter the Slonczewski–Weiss Hamiltonian for graphite.

I. INTRODUCTION

The calculation of the optical properties of solids provide a critical test for any proposed model of the electronic energy bands. There have been several first-principles calculations for the energy bands of graphite that have taken advantage of the nearly two-dimensional nature of this material.[1–3] These models might be expected to fit the high-frequency optical and ultraviolet regions of the graphite optical properties, but they are unsatisfactory in the infrared, where the energy dispersion along the third dimension (c axis) becomes important. A three-dimensional calculation indicates that the agreement with the two-dimensional models at high energies may be fortuitous, since the effects of the dispersion along the third dimension happen to cancel.[3,4] Furthermore, the two-dimensional models do not predict the optical properties, when the electric field of the incident radiation is polarized perpendicular to the basal planes. This paper develops a three-dimensional energy-band model which is valid throughout the Brillouin zone and can be applied to interpret optical data over a wide photon energy range.

The Slonczewski–Weiss–McClure band model for graphite is in the form of a Fourier expansion along the H-K axis of the hexagonal Brillouin zone and a $\vec{k}\cdot\vec{p}$ expansion in the direction normal to this threefold axis.[5–7] This model provides a good description of the Fermi-surface and infrared properties of graphite, which are sensitive to the energy bands near the H-K axis. On the other hand, the optical properties at visible and ultraviolet frequencies are sensitive to a more extended region of the Brillouin zone. The Fourier-expansion technique for electronic energy bands in a periodic solid represents a convenient method for the extension of the $\vec{k}\cdot\vec{p}$ expansions to obtain energy bands valid over the entire zone, thereby permitting calculations of the optical properties associated with the electronic levels over an extensive region of the Brillouin zone. The three-dimensional Fourier expansion developed here reduces to the Slonczewski–Weiss–McClure (SWMcC)[5–7] form along the H-K edge of the Brillouin zone. The Fermi-surface experiments, which have been fitted by the SWMcC model, determine relations between the three-dimensional Fourier-expansion parameters to within a sign. The calculated optical properties implied by the SWMcC model when extended to the full zone can be compared with experiment. The comparison is generally satisfactory, provided the usual[6] sign assignments are made for the SWMcC parameters. In this sense, the present work represents the first verification of the signs of the band parameters γ_0, γ_1, γ_3, and γ_4.

In Sec. II, the three-dimensional Fourier expansion for the graphite structure is developed. An efficient new numerical-integration scheme which is employed for full-zone integrations in the dielectric-constant calculation is given in the Appendix. Results for the dielectric-constant calculation for graphite are given in Sec. III, followed by a discussion of the results in Sec. IV.

II. THREE-DIMENSIONAL FOURIER EXPANSION FOR GRAPHITE

In graphite there are four valence electrons per atom and four atoms per unit cell. These four atoms lie in two layer planes; A, B in the basal plane and A', B' in the neighboring plane.[5] The sp^2 hybrid bonds in the layer planes form three σ-

type electronic energy bands which separate into very low-energy "bonding" and very high-energy "antibonding" states, with a band gap of about 6–12 eV. Near the Fermi energy lie the π bands which are made up from the one leftover p orbital per atom. Thus, at energies somewhat less than the σ-band gap, only the π bands need be considered in calculating the dielectric response function.[8]

To write a general Hamiltonian for the π bands consistent with the graphite crystal symmetry, we choose a basis of four Bloch functions, one for each of the atomic sites within the unit cell. These basis functions may be regarded as generalized tight-binding functions. This derivation is really not restricted to any special basis, since all that is needed for the derivation of the functional form of the Hamiltonian is the correct spatial transformation properties of the eigenfunctions.

If each basis function is associated with a different site, the Hamiltonian may then be written

$$\mathcal{H} = \begin{pmatrix} H_{AA} & H_{AA'} & H_{AB} & H_{AB'} \\ H^*_{AA'} & H_{AA} & H^*_{AB'} & H^*_{AB} \\ H^*_{AB} & H_{AB'} & H_{BB} & H_{BB'} \\ H^*_{AB'} & H_{AB} & H^*_{BB'} & H_{BB} \end{pmatrix} . \tag{1}$$

Taking advantage of the periodicity of the Hamiltonian in k space, the matrix elements of $\mathcal{H}$ can then be expanded in terms of Fourier functions symmetrized according to a given representation of the space group D^4_{6h} for graphite. This same type of procedure has been used previously for the diamond structure.[9] If the distance between two sites i and j is $\vec{d}_{ij}$, then the six independent matrix elements of Eq. (1) are

$$H_{AA}(\vec{k}) = \sum_{d_{AA}}{}' a(\vec{d}_{AA}) F_{1^+}(\vec{k}\cdot\vec{d}_{AA}) , \tag{2a}$$

$$H_{BB}(\vec{k}) = \sum_{d_{BB}}{}' a(\vec{d}_{BB}) F_{1^+}(\vec{k}\cdot\vec{d}_{BB}) , \tag{2b}$$

$$H_{AB}(\vec{k}) = \sum_{d_{AB}}{}' a(\vec{d}_{AB})[F_{1^+}(\vec{k}\cdot\vec{d}_{AB}) + iF_{4^-}(\vec{k}\cdot\vec{d}_{AB})] , \tag{2c}$$

$$H_{AA'}(\vec{k}) = \sum_{d_{AA'}}{}' [a(\vec{d}_{AA'})F_{1^+}(\vec{k}\cdot\vec{d}_{AA'}) + ib(\vec{d}_{AA'})F_{4^-}(\vec{k}\cdot\vec{d}_{AA'})] , \tag{2d}$$

$$H_{BB'}(\vec{k}) = \sum_{d_{BB'}}{}' a(\vec{d}_{BB'}) [F_{1^+}(\vec{k}\cdot\vec{d}_{BB'}) + iF_{4^-}(\vec{k}\cdot\vec{d}_{BB'})] , \tag{2e}$$

$$H_{AB'}(\vec{k}) = \sum_{d_{AB'}}{}' a(\vec{d}_{AB'}) [F_{1^+}(\vec{k}\cdot\vec{d}_{AB'}) - iF_{4^-}(\vec{k}\cdot\vec{d}_{AB'})] , \tag{2f}$$

where $\sum'$ is a sum on inequivalent sites, F_{1^+} and F_{4^-} are the symmetrized Fourier functions given in Table I, and the Fourier-expansion parameters

TABLE I. Symmetrized Fourier functions for the graphite structure. $\xi_x = k_x a$, $\xi_y = (\sqrt{3}) k_y a$, $\xi_z = \frac{1}{2} k_z c$, and $\vec{d}^{nml} = n(a, 0, 0) + m(0, a/\sqrt{3}, 0) + l(0, 0, c/2)$. For graphite $a = 2.46$ Å and $c = 6.74$ Å.

$$F_{1^+}(\vec{k}\cdot\vec{d}^{nml}) = \cos l\xi_z \,[\cos n\xi_x \cos\tfrac{1}{3}m\,\xi_y + \cos\tfrac{1}{2}(n+m)\xi_x \cos\tfrac{1}{2}(n-\tfrac{1}{3}m)\xi_y + \cos\tfrac{1}{2}(n-m)\xi_x \cos\tfrac{1}{2}(n+\tfrac{1}{3}m)\xi_y]$$

$$F_{4^-}(\vec{k}\cdot\vec{d}^{nml}) = \cos l\xi_z \,[\cos n\xi_x \sin(\tfrac{1}{3}m\xi_y) + \cos\tfrac{1}{2}(n+m)\xi_x \sin\tfrac{1}{2}(n-\tfrac{1}{3}m)\xi_y - \cos\tfrac{1}{2}(n-m)\xi_x \sin\tfrac{1}{2}(n+\tfrac{1}{3}m)\xi_y].$$

$a(\vec{d})$ and $b(\vec{d})$ can be shown to be real by time-reversal symmetry. These Fourier coefficients can be interpreted as the matrix elements of the Hamiltonian between Wannier functions, e.g., orthogonalized atomic functions, centered on each lattice site. Our model now has the minimum number of independent coefficients required by symmetry to represent the π band Hamiltonian throughout the Brillouin zone, and explicit values for these parameters may be determined by a fit to a first-principles calculation[10] or by a fit to experimental data.

To evaluate these parameters, we express the Hamiltonian of Eq. (1) in the same basis as is employed in the SWMcC model. This is accomplished by using a unitary transformation that gives the basis functions for $A \pm A'$, B, and B'. Along the Brillouin-zone edge (H-K axis) around which the Fermi surface lies and the SWMcC model applies, the symmetrized Fourier functions can be expanded to first order in $\vec{\kappa} = \vec{k} - \vec{k}_p$, where $\vec{k}_p = (4\pi/3a, 0, k_z)$. The resulting Hamiltonian then reduces to the SWMcC $\vec{\kappa}\cdot\vec{p}$ model.[5–7] McClure[6,11] has shown that seven expansion parameters are satisfactory for the description of Fermi-surface data. The relationship between the Fourier-expansion parameters describing the full-zone band model and the McClure parameters is given in Table II.

Recently, infrared magneto-optical experiments in graphite along with Fermi-surface data have been correlated to provide values for the McClure parameters[12] given in Table III. These values, together with the expressions given in Table II, can provide empirical values for the Fourier-expansion coefficients of the three-dimensional Fourier expansion. As a first approximation in this evaluation procedure, we wished to use as few parameters as possible. Thus only the first terms in each of the expressions in Table II were used. This formulation provides values for the coefficients describing interactions of up to first neighbors in a given plane, and up to two layer planes away. This would be expected to be an adequate

TABLE II. Relation between Fourier coefficients $a(d^{mml}_{\alpha\alpha'})$ and McClure band parameters. $\vec{d}^{mml} = n(a, 0, 0) + m(0, a/\sqrt{3}, 0) + l(0, 0, c/2)$.

$$\gamma_0 = -a(d^{010}_{AB}) + 2a(d^{020}_{AB}) - \tfrac{5}{2}a(d^{120}_{AB}) + \cdots$$
$$\gamma_1 = \tfrac{3}{2}a(d^{001}_{AA'}) + \cdots$$
$$\gamma_2 = 3a(d^{002}_{BB}) + \cdots$$
$$\gamma_3 = \tfrac{1}{2}a(d^{011}_{BB'}) + \cdots$$
$$\gamma_4 = \tfrac{1}{2}a(d^{011}_{AB'}) + \cdots$$
$$\gamma_5 = 3a(d^{002}_{AA}) + \cdots$$
$$\Delta - \gamma_2 + \gamma_5 = 3\,[a(d^{000}_{BB}) - a(d^{000}_{AA})] - \tfrac{3}{2}\,[a(d^{100}_{BB}) - a(d^{100}_{AA})] + \cdots .$$

model if the π orbitals pointed out of the layer plane, minimizing the importance of more distant in-plane neighbors.

We now use the full-zone Fourier expansion to determine the sensitivity of the energy bands at other points in the Brillouin zone to the McClure parameters. A calculation of the optical properties to 7 eV is particularly sensitive to the band structure on the M-L axis, which passes[13] through the center M of the rectangular face of the Brillouin zone and is parallel to the HKH axes at the zone edge. The M-L axis corresponds to the point Q in the two-dimensional Brillouin zone. The optical transition near 5 eV has been assigned[1-4] to the critical points occurring near the M point caused by the saddle-point nature of the energy bands in the basal plane around the M-L axis. The first-term truncation of the Fourier series requires the optical transition at M to occur at about $2\gamma_0$. Using the value of γ_0 deduced from magnetoreflection experiments[12] would predict an optical transition at over 6 eV, whereas the experimentally observed transition is below 5 eV.[4,8] This is clear indication that interactions from more distant in-plane neighbors must be included. By including the first, third, and fourth in-plane neighbors listed in the equation for γ_0 in Table II, we have obtained "effective" values of $\gamma_0 \sim 3.2$ eV along H-K to be consistent with Fermi-surface data and $\gamma_0 \sim 2.3$ eV along M-L to be consistent with optical data. The second and fifth in-plane neighbors do not contribute to γ_0. The energy bands for the π bands of graphite shown in Fig. 1 are determined from the Fourier parameters explicitly written in the equations of Table II, using the Fourier parameter values listed in Table IV. All of the Fourier parameters, except those in the γ_0 expression, directly correspond to the McClure parameters given in Table III. Note that an arbitrary zero of energy can be used to determine one of the "zeroth"-neighbor coefficients in the equation for $\Delta - \gamma_2 + \gamma_5$.

Since we have included the third and fourth in-plane-neighbor interactions, consistency would seem to require that we should use other than the zero values listed in Table IV for the second-neighbor interactions, $a(d^{100}_{AA})$ and $a(d^{100}_{BB})$ which occur in the $\Delta - \gamma_2 + \gamma_5$ expression. Since graphite is nearly two dimensional, one expects the wave functions on the A and B sites to be almost identical, and, therefore, the two second-neighbor interactions should also be nearly identical. Indeed, in a two-dimensional model, symmetry requires that the interactions be equal. Being equal, they would add terms to the three-dimensional Hamiltonian proportional to the unit matrix which would have no effect on the optical properties when only direct transitions are considered. Therefore, the second-neighbor interactions have a negligible effect on the dielectric function, and they have been completely neglected in the present work even though their effect on the electronic energy bands may be larger than many of the other parameters that have been included.

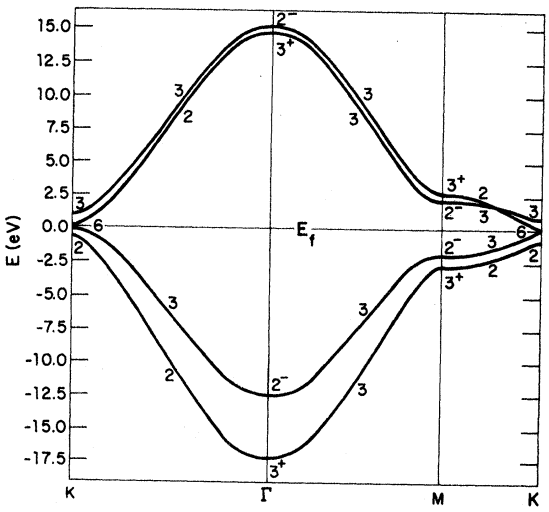

FIG. 1. π energy bands for graphite along several high-symmetry directions. The symmetry labels are according to Ref. 13 for the space group D^4_{6h} (i.e., $P6_3/mmc$). The McClure band-parameter values used are given in Table III; a summary of the corresponding Fourier coefficients is given in Table IV.

TABLE III. Values[a] of the McClure parameters (in eV) used to determine Fourier coefficients.

γ_0	3.18
γ_1	0.40
γ_2	−0.0207
γ_3	0.30
γ_4	0.18
γ_5	−0.006
Δ	0.005

[a]See Ref. 12.

The energy bands of Fig. 1 do not necessarily provide an accurate determination of the density of states. Since the bands were produced by fitting to the optical properties, they provide a satisfactory determination only of the joint density of states. The energy bands would be physically more accurate if values could be found for the second-neighbor interactions. Keeping the interactions nearly equal to avoid disturbing the fit to the optical properties, the electronic energies could be adjusted to match the bandwidths of the π conduction or valence bands, if they could be determined through photoemission or soft x-ray emission experiments, for example. The predicted overlap of the π bands with the σ bands[1-3] makes it very difficult to determine the π bandwidth from the x-ray experiments.[14,15] The 4.7-eV work function in graphite[16] puts most of the π conduction bands below the vacuum level, thus gravely limiting the usefulness of photoemission results[16] to establish only π-band structure. It may be possible to use this technique to study π-σ transitions while using a band model that explicitly includes the σ bands. Recent photoemission experiments[16] have located the valence states at the M point at -1.8 and -2.6 eV below the Fermi level which is less than 10% smaller than our theoretical values of -1.96 and -2.84 eV. A value of ~ -0.2 eV for both second-neighbor interactions would match the photoemission data, but it would not significantly alter the appearance of the energy bands in Fig. 1. For simplicity, we have not added these parameters to our model.

All of the parameters of our model have been evaluated for regions of k space near the rectangular face of the Brillouin zone. Therefore, the greatest errors in the Fourier extrapolation of the Hamiltonian occur at the center of the zone. However, the band structure near Γ is unimportant for a description of the optical properties below ~ 7 eV, because transitions between π bands are forbidden by symmetry at Γ. On the other hand, the σ bands cross the π bands[2,3] near Γ, so that the set of basis functions for the Hamiltonian of Eq. (1) would have to be expanded to include the σ bands, in order to successfully describe the electronic energies in this region of k space. However, it is expected that the σ bands only begin to contribute to the frequency-dependent dielectric constant at frequencies greater than were considered in the present work.

TABLE IV. Values of the Fourier-expansion parameters $a(\vec{d}^{nml})$.

In-plane neighbor No.	Out-of-plane neighbor No.	Parameter	Value (eV)
0	0	$a(d_{AA}^{000})$	0.0069
0	0	$a(d_{BB}^{000})$	0.0136
1	0	$a(d_{AB}^{010})$	−4.20
2	0	$a(d_{AA}^{100})$	0.0
2	0	$a(d_{BB}^{100})$	0.0
3	0	$a(d_{AB}^{020})$	−0.677
4	0	$a(d_{AB}^{120})$	−0.135
0	1	$a(d_{AA}^{001},)$	0.267
1	1	$a(d_{AB}^{011},)$	0.36
1	1	$a(d_{BB}^{011},)$	0.60
0	2	$a(d_{AA}^{002})$	−0.0069
0	2	$a(d_{BB}^{002})$	−0.002

III. CALCULATION OF OPTICAL PROPERTIES

In the relaxation-time approximation, the interband contribution to the dielectric response[17] at absolute zero temperature is

$$\epsilon_{\mu\nu}(\omega) = -\frac{e^2}{\pi^2}\frac{1}{\tilde{\omega}}\sum_{ij}{}'\int_{BZ}\frac{d^3k}{\hbar\omega_{ij}(k)}\left(\frac{\vec{v}_{ij}^{\,\mu}(k)\vec{v}_{ji}^{\,\nu}(k)}{-\tilde{\omega}+\omega_{ij}(k)} - \frac{\vec{v}_{ij}^{\,\nu}(k)\vec{v}_{ji}^{\,\mu}(k)}{\tilde{\omega}+\omega_{ij}(k)}\right), \tag{3}$$

where $\tilde{\omega}=\omega+i/\tau$, $\hbar\omega_{ij}(k)$ is the energy difference $E_i(k)-E_j(k)$, E_F is the Fermi level, and the primed summation is taken over states which satisfy $E_i<E_F<E_j$. The dielectric response function defined in Eq. (3) does not include indirect transitions or any many-body effects. The velocity matrix elements can then be found from the gradient of the Hamiltonian,

$$\vec{v}_{ij}(k)=\{U(k)[\vec{\nabla}_k\mathcal{H}(k)]U^{-1}(k)\}_{ij}, \tag{4}$$

where $U(k)$ is unitary transformation that diagonalizes the Hamiltonian $\mathcal{H}(k)$. The Fourier-expansion Hamiltonian as developed in Sec. II is particularly suitable for a determination of the dielectric response for two reasons. First, the evaluation of the velocity matrix elements using Eq. (4) is quite simple because each Hamiltonian matrix element is a known function of k, and second, the quick evaluation of the energy eigenvalues and velocity matrix elements at many points in the Brillouin zone is facilitated by the small size of the Hamiltonian. Nevertheless, one should be aware that, for a given truncation of the Fourier Hamiltonian, the velocity matrices are not determined as accurately as the energy eigenvalues.

To do the numerical integration over the full Brillouin zone, we divide reciprocal space into small cubes in which the frequency dependence of the integral for each cube may be approximated

by an analytic expression. At first glance, it is not obvious that the various types of Brillouin zones can be divided into cubes without odd pieces sticking out. The hexagonal zone, which must be used for graphite, may be divided by packing cubes together that are standing on their corners; that is, the [111] axis of the cubes is parallel to the c axis of the Brillouin zone. The cube sizes must be fixed so that the rectangular faces of the hexagonal zone contain the centers of any cubes intersected by these faces. Then, the half of a cube protruding from a rectangular face may be reinserted at the rectangular face on the opposite side of the zone that is reached through a translation by a reciprocal-lattice vector. Similarly, the hexagonal face must contain either a cube center or a cube corner with the protrusions and missing pieces fitted in at the opposite hexagonal face. To satisfy these requirements, the c/a ratio for the hexagonal zone must be a rational number times the square root of 2, which can be accomplished by using a simple spatial scaling factor.

Only the subgroup D_{3d} of the full hexagonal point group D_{6h} leaves the cubes invariant. Therefore, it is necessary to integrate over a wedge of $\frac{1}{12}$ of the Brillouin zone instead of the $\frac{1}{24}$ of the zone needed with full hexagonal symmetry. When the crystal being considered, e.g., graphite, has full hexagonal symmetry, the cubes with centers related by a symmetry operation of D_{6h} need to be calculated only once. Other types of Brillouin zones may be divided into cubes by extending the above techniques.

Once the cube locations are established, the accuracy of the integration in Eq. (3) may be improved by subdividing each of a certain set of cubes into 2^3, 3^3, ... smaller cubes. The density and size of the cubes in a particular region of k space is determined by the importance of that region in the determination of the frequency-dependent dielectric constant ϵ. After an expression for the Hamiltonian is developed for the material of interest, matrix elements of the Hamiltonian and its first derivatives with respect to k are calculated at the center of each cube. With this information, a linear extrapolation of the energy eigenvalues is made within each cube. A constant value is approximated for the optical matrix element evaluated using Eq. (4). The linear term in the wave-vector–dependent optical matrix element comes from the second derivative of the Hamiltonian, which is not calculated, to save computer time. Note that the value for the optical matrix element does vary from cube to cube. The contribution to the integral in Eq. (3) from each cube may be formulated analytically with these approximations, by evaluating the expressions presented in the Appendix. As is shown in the Appendix, the evaluation of an integral with spherical, rather than cubic, limits results in a considerable saving of computational time. This time saving enables one to increase the density of cubes to diminsh the error of the linear extrapolation.

The complex dielectric function was calculated from the electronic bands of Fig. 1 for graphite with a constant interband relaxation time of 2×10^{-14} sec. The use of a phenomenological relaxation time allows the simultaneous determination of both the real and imaginary parts of the dielectric response in Eq. (3). The real part of the dielectric response ϵ_1 is more sensitive to the relaxation time. Thus, the final value of the relaxation time was chosen to match the experimental behavior[8] of ϵ_1 near the 5-eV critical point. This value for the interband relaxation time agrees with values found in other materials.[9,18,19]

In performing the momentum-space integration, over 1200 grid points with high concentrations near the H-K-M-L face were used in $\frac{1}{24}$ of the Brillouin zone. The rest of the Brillouin zone was accounted for by using appropriate weighting factors for each grid point, which were determined by symmetry considerations. For the electric field polarized in the basal plane ($\vec{E}\perp\vec{c}$), our theoretical values for the interband dielectric constant (dark curve in Fig. 2) compare favorably with the Kramers–Kronig analysis of normal incidence reflectivity data[8] (light curve shown in Fig. 2). The low-frequency contribution is primarily from the H-K axis of the Brillouin zone, while the structure near 5 eV is from the M-L axis. The contribution of the σ bands to the dielectric constant for the energy range shown in Fig. 2 has been modeled as a frequency-independent core value of 1.5, following the separation of the dielectric response into π and σ regions, as was carried out by Taft and Philipp.[8] Including the contribution of free space, a total core dielectric constant of 2.5 has been added to ϵ_1 in Fig. 2(a).

The discrepancy between the experimental and the solid theoretical curves for $\epsilon_1^{\perp}(\omega)$ and $\epsilon_2^{\perp}(\omega)$ which appears in Fig. 2 at low photon energies is largely due to the free-carrier contribution to the total dielectric response. The free-carrier contribution is calculable, in principle, from an integral over the Fermi surface as determined by the SWMcC model.[5–7] This calculation has not yet been done for the values of the McClure parameters in Table III. An approximate treatment of the free-carrier contribution can be given by estimating the plasma frequency ω_p associated with the free carriers from the effective masses of the model. This gives a value for ω_p of approximately 0.5–1.0 eV for $\vec{E}\perp\vec{c}$, and about an order of magnitude less for $\vec{E}\parallel\vec{c}$. For photon energies above 1 eV, free-carrier contributions are probably not important

for either polarization. We have added the free-carrier contributions to the dielectric response to produce the dashed curve in Fig. 2 through the use of a Drude[20] term of the form $-\omega_p^2/\omega(\omega+i/\tau)$. The value of ω_p that fitted the experimental data best was about $\hbar\omega_p = 0.95$ eV for $\vec{E}\perp\vec{c}$. This agrees with the dc conductivity measurements[21,22] if the low-frequency intraband relaxation time is just over 10^{-13} sec, which is almost an order of magnitude larger than the interband relaxation time. The substantial free-carrier contribution at low photon energies accounts for the negative experimental values of ϵ_1, observed for $\vec{E}\perp\vec{c}$, at low energies, as shown in Fig. 2(a). Furthermore, the free-carrier contribution produces a positive divergence in ϵ_2 at low frequencies for $\vec{E}\perp\vec{c}$ and also for $\vec{E}\parallel\vec{c}$.

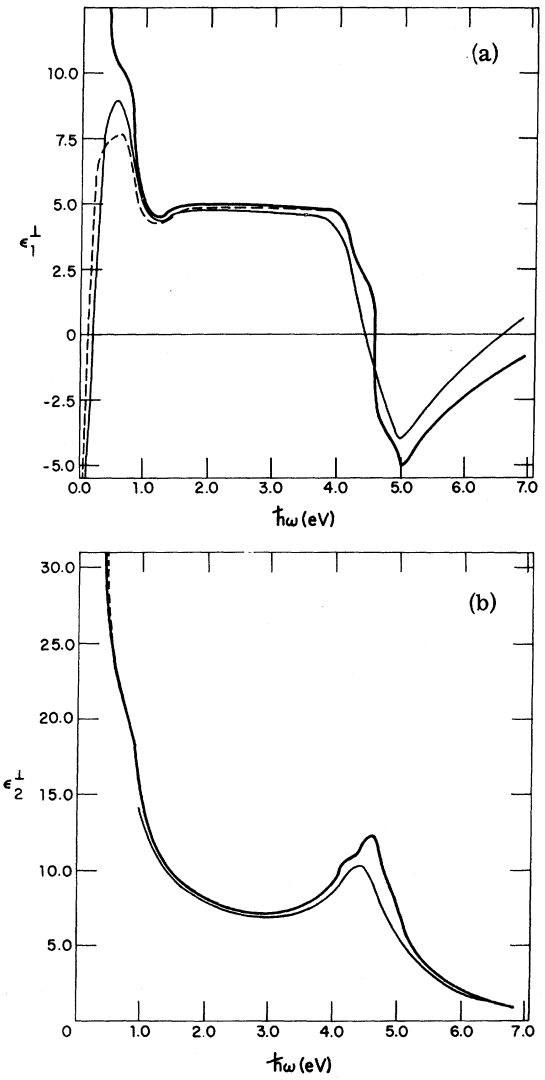

FIG. 2. Calculated interband dielectric response $\epsilon^\perp(\omega)$ for $\vec{E}\perp\vec{c}$ (dark curve). A Drude term was added with a free-carrier plasma frequency of $\hbar\omega_p = 0.95$ eV (dashed curve). The experimental data (light curve) are from Taft and Philipp (Ref. 8). The core contribution to $\epsilon_1^\perp(\omega)$ is taken as 2.5.

As the frequency goes to zero, the present calculation of the interband contributions to the dielectric function becomes infinite, similar to the prediction of the two-dimensional band models.[2] This occurs in semimetals when the conduction and valence bands intersect at the Fermi level so that the hole Fermi surface in the valence band touches the electron Fermi surface in the conduction band. If the Fermi surfaces intersect on a line or in a plane, the zero band gap between the initial and final states causes an infinite contribution to the dielectric response [see Eq. (3)] similar to that for the free carriers. The linear extrapolation can only have planar constant-energy surfaces which intersect along a line so that a logarithmic singularity in the joint density of states results. Thus, there would seem to be a nonzero interband contribution to the dc conductivity from the zero-frequency limit of ϵ_2. In graphite, the band degeneracy along H-K which produces the vanishing band gap is lifted by the spin-orbit interaction,[7] which is expected to be $\sim 10^{-4}$ eV in magnitude.[23] Below this energy range, the interband contribution to the conductivity would fall toward zero as one would expect. Since the spin-orbit splitting has a negligible effect on the optical properties in the energy range of interest in the present treatment, it has been neglected in the development of the energy-band model. Still, we must use a high density of cubes around the H-K axis to reduce the error of the linear extrapolation for small band gaps (see the Appendix).

Although various attempts have been made to study the optical properties of graphite for $\vec{E}\parallel\vec{c}$ in the photon energy range below 6 eV,[4,24] only scanty experimental data are currently available for a quantitative description of the large anisotropy of the optical constants. Predictions of $\epsilon^{\parallel}(\omega)$ based on the energy-band model of Fig. 1 are given in Fig. 3 for both $\epsilon_1^{\parallel}(\omega)$ and $\epsilon_2^{\parallel}(\omega)$. In constructing this figure, a core dielectric constant of 1 was used, which includes only the free-space contribution. The dashed curves again incorporate the free-carrier contributions with a Drude term. We have used a free-carrier plasma frequency of 0.1 eV in agreement with the two orders of magnitude anisotropy observed experimentally in the dc conductivity.[21,22] Experimental problems, discussed in Sec. IV, could make it difficult to observe the predicated dependence for $\vec{E}\parallel\vec{c}$ shown in Fig. 3. The structure around 4.3 eV is not associated with any critical point, since it comes from an extended volume of the Brillouin zone near the L point, but displaced towards the H-K axis. This differs from

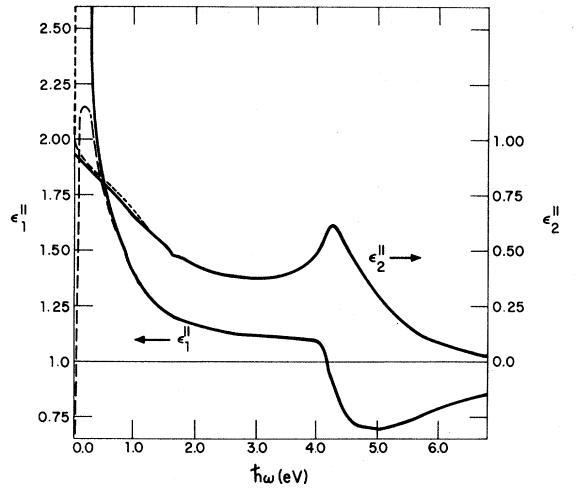

FIG. 3. Dielectric response for $\vec{E} \parallel \vec{c}$. Here the free-carrier plasma frequency is taken as $\hbar\omega_p = 0.1$ eV and the core contribution to $\epsilon_1^{\parallel}(\omega)$ is taken as 1.0.

the results obtained for $\vec{E} \perp \vec{c}$, where there are large contributions in the photon energy range between 4 and 5 eV from a volume centered around the critical point at M, as well as from a volume around the L point.

IV. DISCUSSION

The present treatment not only calculates the graphite optical properties from a three-dimensional model that goes beyond the SWMcC model; it also includes the k dependence of the optical matrix elements. The method of k-space integration developed in the Appendix facilitates the quick and accurate determination of both the real and imaginary parts of the frequency-dependent dielectric constant. The integration scheme requires that the Hamiltonian must be diagonalized at many points in the Brillouin zone. Thus, the Fourier-expansion technique, as used in Sec. II, provides a convenient representation for the Hamiltonian by giving an analytic expression for the Hamiltonian valid throughout the Brillouin zone. Also, the dimension of the Hamiltonian is much smaller than that normally used in other representations, e.g., the plane-wave representation for a pseudopotential calculation. Therefore, the time required to diagonalize the Hamiltonian may be kept to a minimum. The same procedure has recently been extended to calculate the optical properties of arsenic[25] and tellurium.[26]

The π bands in graphite in Fig. 1 are determined from the McClure parameters that fit the infrared magneto-optical and Fermi-surface data[12] along with the addition of in-plane neighbor interactions so that the allowed optical transitions at M occur near 5 eV. Unfortunately, the signs of the McClure parameters are somewhat ambiguous because the SWMcC Hamiltonian is invariant under changing the signs of several subsets of the McClure parameters. The signs of the parameters have already been adjusted[27] to have electrons rather than holes at the K point. At the M point several possible band orderings may be obtained from the truncated Fourier expansion by appropriate adjustments of the signs of the McClure parameters while leaving the SWMcC Hamiltonian invariant. In order to give the single reflectivity peak observed experimentally,[4,8] the allowed optical transitions between states of opposite parity must have nearly the same energy. This eliminates many of the possible sign changes. To justify the sign assignments of Table III, we can resort to physical arguments that take advantage of the direct relationship of the Fourier coefficients to matrix elements of the Hamiltonian in the Wannier representations. A positive value for γ_0 is taken since it represents, primarily, the negative of the nearest-neighbor interaction which is expected to be attractive because the electrons are relatively free to move about in the basal planes. An argument similar to that for γ_0 implies that γ_1 should remain positive. The only other McClure parameters important in the determination of the dielectric function in the optical region are γ_3 and γ_4. The signs of these parameters are more difficult to estimate since they represent out-of-plane interactions. To obtain a state of even parity as the lowest-energy state at the Γ point, γ_3 must be positive. With the previous three sign assignments, the magneto-optical and Fermi-surface data can only be fitted by a positive value of γ_4. With γ_4 positive; a band crossing occurs in the conduction bands between K and M (see Fig. 1) in agreement with previous calculations.[3,4] A crossing of the valence or conduction bands is required to reverse the parity ordering of the states between the M and K points to agree with the optical experiments. The calculation of the frequency-dependent dielectric constant is insensitive to whether or not there is a conduction or a valence-band crossing; so, based on optical data, we cannot say with certainty in which bands the crossing occurs. Crossing conduction bands are consistent with the physical arguments we have presented for the usual[6,11] signs of the McClure parameters whose magnitudes were found in Ref. 12.

To extend the range of validity of our model to higher photon energies, the σ bands must be included. This project could be made simpler by neglecting the three-dimensional splitting of the σ bands, which is probably much smaller than for the π bands. Thus, the previous two-dimensional calculations may give sufficiently reliable results for the σ bands. Bassani and Parravicini[2] give a

6-eV separation of the σ conduction and valence bands. Thus, the allowed transition between the σ bands at Γ for this energy would have to be many times weaker than the observed π band transitions at 4.8 eV, since there is no significant structure observed in the optical properties with electric field in the basal plane at 6 eV. Greenaway *et al.*[4] maintain that there is a slight shoulder in the reflectivity just above 6 eV. However, we can produce an asymmetry in the usual 4.8-eV π band peak that looks very similar to the shoulder by modeling the σ band contribution as a real frequency-independent core value of 1.5 in the dielectric response. On the other hand, Painter and Ellis[3] obtain a 12-eV separation of the σ bands. This larger separation of the σ bands could produce the increase in ϵ observed by Taft and Philipp[8] above 10 eV, and is more consistent with the photoemission data[16] and our ability to model the low-frequency optical properties with only π bands. Plasma effects are also very important in the high-photon-energy region.[28,29]

We have shown in Fig. 2 that the optical properties of graphite can be predicted for the electric field polarized in the basal plane by a semiempirical Fourier-expansion model. The good agreement between theory and experiment is extended to low frequencies when the free carriers are taken into account through a simple Drude dependence. The energies of the three-dimensional band structure used are in qualitative agreement with the π bands derived in previous first-principles band structures, such as those of Painter and Ellis[3] or Bassani and Parravicini.[2] The general description given by Painter and Ellis of their three-dimensional results seems applicable to the energy bands of Fig. 1, except that the present calculation has energy bands along *HKH*, as given in Ref. 27, that produce electrons at the *K* point. Painter and Ellis did not test their model with a calculation of the optical properties. Bassani and Parravicini did, however, calculate the joint density of states, using a constant-matrix-element approximation, and their two-dimensional result showed a much sharper structure than is observed experimentally in the optical properties. A later paper[4] determined the three-dimensional corrections to the band structure, which found crossing conduction bands between *M* and *K* in agreement with our results. In another treatment of the optical properties, Kobayashi and Uemura[30] and Imatake and Uemura[31] attempted to extend the SWMcC model using only γ_0 and γ_1 to explain the 4.8-eV peak in the optical properties with $\vec{E} \perp \vec{c}$. The calculated optical properties contained two transitions separated by 1.6 eV, because these authors obtained a different energy-band ordering at *M*. In order to successfully extrapolate to the *M*-point energies, we find that at least the McClure parameters γ_0, γ_1, γ_3, and γ_4 must be used. Since the SWMcC model is only valid near the *H*-*K* axis, it is not surprising that to adequately describe the optical properties more parameters need to be added to the set originally used by McClure.[6,11] Up to the fourth neighbor, interactions in the basal plane must be included in our model (see Table IV) to reconcile the 3.2-eV value of γ_0 provided by the low-frequency magneto-optical and Fermi-surface data with the value of 2.3 eV required for a fit to the optical data at higher frequencies.

We have given the first theoretical determination of the optical properties in Fig. 3 with the electric field polarized perpendicular to the basal planes ($\vec{E} \parallel \vec{c}$). The experimental observation of the optical reflectivity for this polarization is severely restricted by the difficulty of preparing a suitable optical-crystal face perpendicular to the basal planes. Ergun[24] has measured the reflectivity as a function of polarization on faces inclined at 58° to the basal planes which occur in natural single crystals of graphite. He observes a reflectivity with $\vec{E} \parallel \vec{c}$ of just less than 10% with no structure between 2 and 5 eV. The non-normal incidence experiments[4] on the basal plane yield similar results with a somewhat smaller value for the reflectivity. This contrasts with our prediction of a very small reflectivity except near 4.3 eV, where Fig. 3 indicates a reflectivity peak. Our results are admittedly more inaccurate for this polarization, but it seems unlikely that the reflectivity for this polarization could be as large as has been measured[4,24] without some structure. To get a reflectivity of nearly 10% would require a core contribution of well over 3.0, which seems too high to be associated with the high-energy σ-π transitions. It could be that experimental difficulties have prevented the observation of the very large anisotropy (about an order of magnitude) that we predict. For example, a slight depolarization of the light in either experiment[4,24] would wash out structure in the measured reflectivity with $\vec{E} \parallel \vec{c}$.

On the other hand, structure has been observed in modulated reflectivity measurements and perhaps can be associated with the polarization $\vec{E} \parallel \vec{c}$. Recent thermoreflectance[32] data have shown considerable structure around 4.5 eV; these data were taken for unpolarized light at a 45° angle of incidence to the basal planes, which would therefore include effects from both polarizations, $\vec{E} \perp \vec{c}$ and $\vec{E} \parallel \vec{c}$. An earlier experiment[33] at near-normal incidence which would measure only $\vec{E} \perp \vec{c}$ did not reveal any structure below the main 4.8–5-eV transition. One may speculate that some of the 4.5-eV structure may be associated with our predicted peak in the optical properties with $\vec{E} \parallel \vec{c}$. It would be interesting to carry out an experiment

to look for anisotropy in the observed thermoreflectance structure.

ACKNOWLEDGMENTS

The authors wish to gratefully acknowledge many helpful suggestions and discussions with Professor M. S. Dresselhaus. The comments of Professor J. W. McClure are also deeply appreciated.

APPENDIX: MOMENTUM-SPACE INTEGRATION TECHNIQUE

After doing a partial-fraction expansion of Eq. (3), the linear extrapolation as discussed in Sec. III makes it necessary to evaluate the following type of integrals over a small momentum-space cube centered about $\vec{k}_0$, with length Δ_k along a cube edge:

$$I_c(\vec{k}_0) = M(\vec{k}_0)\int_{\text{cube}} \frac{d^2\kappa}{\beta(\vec{k}_0)+\vec{\alpha}(\vec{k}_0)\cdot\vec{\kappa}}$$

$$= \frac{M(\vec{k}_0)}{2\Pi_m \alpha_m(\vec{k}_0)} [\beta(\vec{k}_0)+\vec{\alpha}(\vec{k}_0)\cdot\vec{\kappa}]^2 \times \ln[\beta(\vec{k}_0)+\vec{\alpha}(\vec{k}_0)\cdot\vec{\kappa}]\Big|_{-\Delta_2/2}^{\Delta_k/2}, \quad \text{(A1)}$$

where $M(\vec{k}_0)$ is a constant function of the matrix elements,

$$\vec{\kappa} = \vec{k} - \vec{k}_0, \quad \beta(\vec{k}_0) = \omega_{ij}(\vec{k}_0) + \begin{Bmatrix} \tilde{\omega} \\ -\omega \\ 0 \end{Bmatrix},$$

which is different for each of the three terms of the partial function expansion, and $\alpha_m(\vec{k}_0) = \partial\beta(k)/\partial k_m\big|_{\vec{k}=\vec{k}_0}$, in which $m = 1, 2, 3$ are the vector components. Note that $\beta(\vec{k}_0)$ may be complex, but the $\alpha_i(\vec{k}_0)$ are all real. A significant difference between this and previous linear-extrapolation techniques is the use of the interband relaxation time which eliminates the need for taking principal values of infinite integrals.[34] Also, the relaxation time makes it possible to calculate simultaneously both the real and imaginary parts of the dielectric response.

The higher-order terms in κ, which were omitted in Eq. (A1), may be represented by including the effects of the second derivative of the Hamiltonian. Let us define $\overleftrightarrow{K}$ as the curvature of the frequency difference $\omega_{ij}(k)$,

$$\overleftrightarrow{\kappa}^{ij}(k) = \vec{\nabla}_k\vec{\nabla}_k\omega_{ij}(k) = \vec{\nabla}_k\vec{\nabla}_k[E_i(k) - E_j(k)]/\hbar. \quad \text{(A2)}$$

Including these curvature terms, the integral of Eq. (A1) becomes

$$I_s(\vec{k}_0) = M\int \frac{d^3\kappa}{\beta+\vec{\alpha}\cdot\vec{\kappa}} \frac{1}{1+\vec{\kappa}\cdot\overleftrightarrow{K}\cdot\vec{\kappa}/(\beta+\vec{\alpha}\cdot\vec{\kappa})},$$

where $\vec{\alpha}$, β, and $\overleftrightarrow{K}$ are evaluated at $\vec{k}_0$. Therefore, the error for a given optical transition is small if

$$\Delta_k^2 \ll \frac{\beta}{\sum_{\mu\nu}|\overleftrightarrow{K}^{ij}_{\mu\nu}|}; \quad \text{(A3)}$$

that is, the ratio of the curvature of the energy difference to the band gap must be small. This requirement can present problems in the low-frequency region where regions of k space with small band gaps make the primary contributions to the dielectric response. The calculation of ϵ for graphite is especially sensitive to these restrictions, since there are several points in k space near the H-K axis where the band gap nearly goes to zero between occupied and unoccupied states.[6]

A valid criticism of this and other linear-expansion techniques is that it is not accurate around critical points; i.e., the bands may be nearly parallel around a critical point, and the linear expansion may extrapolate the "parallelness" to a very large volume, thereby overestimating the resonance in ϵ. This can be avoided to a certain extent by a judicious placement of the cube (or sphere) centers, so that they do not lie on high-symmetry points of the Brillouin zone. One can then resort to increasing the density of the cubes to achieve any desired accuracy. Even near critical points, our experience has indicated that considerably fewer points, i.e., cubes or spheres, need be used in this scheme than in a Monte Carlo integration, for example.

Because κ_x, κ_y, and κ_z each have to be evaluated at both limits, Eq. (A1) requires that the complex logarithm be evaluated eight times for each term in the partial-fraction expansion for every cube. The computer time needed may be significantly reduced if the cube integral is approximated by an integral over a sphere of equal volume having radius $R = (3/4\pi)^{1/3}\Delta_k$:

$$I_s(k_0) = M(\vec{k}_0)\int_{\text{sph}} \frac{d^3\kappa}{\beta+\vec{\alpha}\cdot\vec{\kappa}}$$

$$= \frac{\pi M(\vec{k}_0)}{\alpha^3}\left((\beta^2-\alpha^2R^2)\ln\frac{\beta-\alpha R}{\beta+\alpha R} + 2\beta\alpha R\right), \quad \text{(A4)}$$

in which $\vec{\alpha}$ and β are evaluated at $\vec{k}_0$ and the scalar quantity $\alpha(\vec{k})$ denotes the amplitude of the corresponding vector quantity. The major advantage of the integration over a sphere is that the logarithm term of Eq. (A4) has to be evaluated only once as compared with eight times in Eq. (A1), thereby achieving a considerable saving in computer time. A comparison of the approximation schemes of Eqs. (A1) and (A4) applied to graphite showed that they differed by less than 5% in a determination of the dielectric-response function using a 100-cube subdivision of the Brillouin zone; the spherical approximation used only $\frac{1}{6}$ of the computer time needed when integrating over the whole cube. A

more detailed discussion of the error introduced by the spherical approximation is given in the doctoral dissertation of one of the authors.[35] The time advantage of the spheres may be used to reduce the error of the linear approximation by taking a high density of spheres in the same amount of time that it takes to integrate over fewer cubes.

For the case of metals and semimetals, the Fermi-level cutoff provides additional complications in setting the limits on the integrals in Eq. (A1) or Eq. (A4). The spherical approximation still has an analytic expression when the energy bands cross the Fermi level. Consider the contribution to the dielectric response from a transition between two bands, one of which crosses the Fermi level. As a consequence of the linear approximation to the energy bands, all constant-energy surfaces are represented by a series of planes inside the region of integration. Using spherical coordinates with the z axis perpendicular to the Fermi surface, the needed integral is

$$I_s'(z_0, k_0) = M(k_0) \int_{z_0}^{R} d\kappa \int_0^{\theta_0} d\theta \int_0^{2\pi} d\varphi \, \frac{\kappa^2 \sin\theta}{\beta + \vec{\alpha}\cdot\vec{\kappa}} , \tag{A5}$$

where z_0 is the distance from the center of the sphere to the Fermi surface, $\theta_0 = \cos^{-1}(|z_0|/\kappa)$, and $\vec{\alpha}$ and β are defined below Eq. (A1). After using the method of residues to evaluate the integral over φ, the rest of the integration of (A5) is straightforward, and one obtains

$$I_s'(z_0, k_0) = \frac{\pi M}{\alpha^3}\left((\beta^2 - \alpha^2 R^2) \ln \frac{\beta\alpha_3 + \alpha^2 z_0 + \alpha S}{(\alpha_3 + \alpha)(\beta + \alpha R)} + \beta\alpha(R - z_0) + \frac{\alpha(\beta\alpha_3 + \alpha^2 z_0)}{\alpha^2 - \alpha_3^2}\left[S - (\beta + \alpha_3 z_0)\right]\right), \tag{A6}$$

where

$$S = \pm\left[(\beta + \alpha_3 z_0)^2 - (R^2 - z_0^2)(\alpha^2 - \alpha_3^2)\right]^{1/2}, \tag{A7}$$

and α_3 is the projection of difference in energy gradients of the two bands $\vec{\alpha}$ onto the energy gradient of the crossing band. The dependence of α, β, and α_3 on k_0 has been suppressed in writing Eqs. (A6) and (A7) for simplicity. By carefully keeping track of the region of physical values of the variables, one can establish that the sign of the complex root in Eq. (A7) should be such that the root is always in the same quadrant as $\beta + \alpha_3 z_0$. Similarly, the physical branch of the logarithm can be shown to have no multiples of $2\pi i$ added, and the branch cut is along the negative real axis. Note that

$$\lim I_s'(z_0) = I_s \quad \text{as} \quad z_0 \to -R, \tag{A8}$$

where I_s is the spherical integral with no Fermi-level intersection as defined in Eq. (A4).

Even when two bands cross the Fermi level in the same sphere, Eq. (A6) may be used to derive an analytic expression for the required integral for the diagonal components of the dielectric tensor $\epsilon_{\mu\mu}$. However, for small band gaps between strongly interacting bands, the linear extrapolation may represent the bands as crossing each other at or near the Fermi level, which produces an infinite or inordinately large contribution to the dielectric response. To avoid crossing bands at the Fermi level, we have not included contributions from transitions between energy bands when both their linear extrapolations cross or nearly cross the Fermi level within one of the small cubes. The error introduced by the elimination of these types of transitions can be made small by further subdivision of the cubes where the error occurs, so that no more than one band crosses the Fermi level in most of the smaller cubes.

*Work sponsored by the Department of the U. S. Air Force and the National Science Foundation.

†NSF Predoctoral Fellow. Present address: Dept. of Physics, University of Oregon, Eugene, Ore.

[1]F. J. Corbato, in *Proceedings of the Third Conference on Carbon* (Pergamon, London, 1959), p. 173; Ph.D. thesis (MIT, 1956) (unpublished).

[2]F. Bassani and G. Parravicini, Nuovo Cimento 50, 95 (1967).

[3]G. S. Painter and D. E. Ellis, Phys. Rev. B 1, 4747 (1970).

[4]D. L. Greenaway *et al.*, Phys. Rev. 178, 1340 (1969).

[5]J. C. Slonczewski and P. R. Weiss, Phys. Rev. 109, 272 (1958).

[6]J. W. McClure, Phys. Rev. 108, 612 (1957).

[7]G. Dresselhaus and M. S. Dresselhaus, Phys. Rev. 140, A401 (1965).

[8]E. A. Taft and H. R. Philipp, Phys. Rev. 138, A197 (1965).

[9]G. Dresselhaus and M. S. Dresselhaus, Phys. Rev. 160, 649 (1967).

[10]J. C. Slater and G. F. Koster, Phys. Rev. 94, 1498 (1954).

[11]J. W. McClure, Phys. Rev. 119, 606 (1960).

[12]B. L. Heflinger and M. S. Dresselhaus (unpublished); B. L. Heflinger, M. S. thesis (MIT, 1971) (unpublished).

[13]S. C. Miller and W. F. Love, *Tables of Irreducible Representations of Space Groups and Co-Representations of Magnetic Space Groups* (Pruett, Boulder, Colo., 1967).

[14]C. F. Chalklin, Proc. Roy. Soc. (London) A194, 42 (1948).

[15]T. Sagawa, J. Phys. Soc. Japan 21, 49 (1966).

[16]R. F. Willis, B. Feuerbacher, and B. Fitton, Phys. Rev. B 4, 2441 (1971).

[17]H. Ehrenreich and M. H. Cohen, Phys. Rev. 115, 786 (1959).

[18]G. Dresselhaus, M. S. Dresselhaus, and D. Beaglehole, in Electronic Density of States, NBS Special Bulletin No. 323, edited by L. H. Bennett, 1971, p. 33 (unpublished).

[19]B. R. Cooper, H. Ehrenreich, and H. R. Philipp, Phys. Rev. 138, A494 (1965).
[20]P. Drude, *The Theory of Optics* (Longmans, Green and Co., New York, 1902).
[21]W. Pimak and L. H. Fuchs, Phys. Rev. 95, 22 (1954).
[22]W. Primak, Phys. Rev. 103, 544 (1956).
[23]J. W. McClure and Y. Yafet, in *Proceedings of the Fifth Carbon Conference* (Pergamon, Oxford, England, 1962), p. 22.
[24]S. Ergun, in *Chemistry and Physics of Carbon*, edited by P. L. Walker, Jr. (Marcel Dekker, New York, 1968), Vol. 3, p. 45.
[25]R. L. Brodersen, Ph.D. thesis (MIT, 1972) (unpublished).
[26]G. Dresselhaus (unpublished).
[27]P. R. Schroeder, M. S. Dresselhaus, and A. Javan, Phys. Rev. Letters 20, 1292 (1968).
[28]H. R. Philipp, in *Optical Properties and Electronic Structure of Metals and Alloys*, edited by F. Abelès (Wiley, New York, 1966), p. 408.
[29]E. Tosatti and F. Bassani, Nuovo Cimento 65, 161 (1970).
[30]K. Kobayashi and Y. Uemura, J. Phys. Soc. Japan 25, 404 (1968).
[31]A. Imatake and Y. Uemura, J. Phys. Soc. Japan 28, 410 (1970).
[32]M. Anderegg, B. Feuerbacher, and B. Fitton, Phys. Rev. Letters 26, 760 (1971).
[33]A. Balzarotti and M. Grandolfo, Phys. Rev. Letters 20, 9 (1968).
[34]G. Gilat and L. J. Raubenheimer, Phys. Rev. 144, 390 (1966).
[35]L. G. Johnson, Ph.D. thesis (MIT, 1973) (unpublished).

PHYSICAL REVIEW B VOLUME 7, NUMBER 6 15 MARCH 1973

Localized Basis for Lattice Vibrations*

W. Kohn
Department of Physics, University of California, San Diego, La Jolla, California 92037
(Received 12 October 1972)

For the case of electrons in a periodic lattice there exist extended basis functions (Bloch waves) and localized basis functions (Wannier functions). It is shown here that also for lattice vibrations there exists, in addition to the usual extended basis functions (normal modes), a set of localized basis functions. These are nontrivial only for lattices with several atoms per unit cell. Examples are worked out and discussed. These functions appear to be of interest for the treatment of defects and other problems calling for a localized description.

The electronic theory of solids has been largely developed in the language of Bloch functions, which are extended throughout the entire solid. While this approach has generally been eminently appropriate and successful, it has one drawback: The effective interactions between electrons are generally of short range and many interesting phenomena in solids, such as those associated with defects, are of a local character. For some purposes it is therefore somewhat unnatural, and also an obstacle to the application of physical or chemical intuition, to work in a representation of infinitely extended states. This drawback can be overcome by the use of localized Wannier functions[1] which span the same space as the extended Bloch functions.

For similar reasons it appears to be of interest to construct a localized orthonormal basis for lattice vibrations, which spans the same space as the well-known delocalized normal modes of the crystal lattice.[2] This will be done in the present paper.

The localized basis to be discussed is nontrivial only for lattices with more than one atom per unit cell. We therefore consider first a diatomic lattice in one dimension with lattice parameter a, masses M_1 and M_2, and two nearest-neighbor force constants α and β. The N lattice cells (with $N\to\infty$) are labeled by $l=-\frac{1}{2}N,\ldots,+\frac{1}{2}N-1$; and the two atoms in each cell by $\kappa=1,2$ (see Fig. 1). It is well known[3] that the atomic displacements in a normal mode of vibration of wave number k and frequency ω have the form

$$w_{l,\kappa}=M_\kappa^{-1/2}u_\kappa e^{i(kla-\omega t)}, \tag{1}$$

where the coefficients u_κ satisfy the equations

$$\omega^2 u_\kappa(k)=\sum_{\kappa'=1}^{2} D\begin{pmatrix}k\\ \kappa\kappa'\end{pmatrix}u_{\kappa'}(k)\,; \tag{2}$$

and the matrix

$$D\left(\begin{smallmatrix}k\\ \kappa\kappa'\end{smallmatrix}\right)\equiv\begin{pmatrix}\dfrac{\alpha+\beta}{M_1} & \dfrac{\alpha+\beta e^{-ika}}{(M_1M_2)^{1/2}}\\[2ex] \dfrac{\alpha+\beta e^{ika}}{(M_1M_2)^{1/2}} & \dfrac{\alpha+\beta}{M_2}\end{pmatrix}. \tag{3}$$

The eigenfrequencies are given by the quadratic secular equation

$$\left|D\begin{pmatrix}k\\ \kappa\kappa'\end{pmatrix}-\omega^2(k)\,\delta_{\kappa\kappa'}\right|=0\,, \tag{4}$$

whose two solutions for each value of k are denoted by $\omega^2\left(\begin{smallmatrix}j\\ k\end{smallmatrix}\right)$ $(j=1,2)$. These constitute the acoustic